Theory and Design of Frequency-Tunable Absorptive Bandstop Filters

Mark D. Hickle, *Member, IEEE*, and Dimitrios Peroulis, *Fellow, IEEE*

***Abstract*— Absorptive bandstop filters are a relatively new class of bandstop filter, which are able to achieve very high levels of stopband rejection with relatively low-quality-factor resonators, in contrast to typical reflective bandstop filters, whose stopband rejections are limited by the quality factors of their resonators. This paper performs an in-depth theoretical and practical analysis of this class of filter, presenting design principles for reducing the sensitivity to process variation, increasing the tuning range over which the filters can operate with good performance, and addressing the practical non-ideal effects of implementation, such as frequency variation of couplings and quality factor. Four varactor-tuned microstrip bandstop filters are presented to verify the presented theory. They illustrate the design tradeoffs between selectivity and tuning range, choice of coupling topology and tuning range, and show the benefits and drawbacks of cascading stages to create higher-order filters.**

***Index Terms*— Filters, microstrip filters, resonator filters, tunable circuits and devices.**

I. Introduction

ONE of the main attractive features of cognitive radio transceivers is their ability to dynamically adjust operation parameters such as center frequency, bandwidth, and modulation type, in order to optimally utilize the available spectrum [1]. Such transceivers often maximize frequency flexibility by utilizing very wideband RF front ends, but this leaves the receiver prone to jamming signals which can saturate the receiver and block the desired signals of interest. These jamming signals can come from a variety of intentional or unintentional sources, and are often dynamic, unpredictable, and can be many orders of magnitude stronger than the signals of interest. Tunable bandstop filters, which have the ability to dynamically suppress a narrow band of frequencies while maintaining a wide passband, offer a potential solution to this problem and, as a result, have garnered much research interest in recent years. One particular drawback of tunable bandstop filters, however, is that tunable resonators in compact form-factors tend to have low unloaded quality factors (Q_U). Since the amount of attenuation that a typical bandstop filter can achieve is limited when low-quality-factor resonators are used, many of the published tunable bandstop filters fail to provide the high levels of rejection that are needed in cognitive radio applications.

A bandstop filter utilizing evanescent-mode cavity resonators is presented in [2]. Its maximum attenuation only ranges from 15–35 dB with a 1.2% to 3.2% fractional bandwidth. In [3] a varactor-tuned micostrip bandstop filter is demonstrated with 37–40 dB of stopband attenuation for a fractional bandwidth of 10%–14 %. Stopband rejection of 7–27 dB with a fractional bandwidth of 1.6%–3.6% is presented in [4], which is a bandstop filter implemented with varactor-tuned substrate-integrated evanescent-mode cavity resonators. Other notable examples of tunable bandstop filters can be found in [5]–[7].

Two other notable, relatively recent types of bandstop filters are the N-path filter [8], [9] and the transversal signal-interference filter [10]. N-path filters have the advantage of being fully integrated on-chip, can have very narrow bandwidths, and can be very widely tunable. However, their ultimate stopband rejection is limited to around 25 dB [8]. Transversal signal-interference filters are able to provide very sharp stopbands with high levels of rejection, but in general are not amenable to tunability since their center frequencies are determined by electrically-long lengths of transmission line.

A new class of bandstop filter which partially overcomes the aforementioned problems caused by low-quality-factor resonators was recently introduced in [11]–[13]. This type of filter achieves its stopband attenuation not by reflecting incident signals as traditional reflective bandstop filters do, but by utilizing two signal paths which are 180° out of phase and result in destructive interference over a narrow bandwidth. This allows the filter to achieve very large (theoretically infinite) attenuation in its stopband, regardless of the constituent resonators' unloaded quality factors. This kind of filter is called an "absorptive bandstop filter" because it realizes its increased stopband attenuation by absorbing a portion of the incident signals which would otherwise be reflected, although it is not restricted to being perfectly absorptive and can have both zero and non-zero reflection coefficients in its stopband. The concept has been utilized by several authors since, and has been demonstrated in technologies

Manuscript received April 30, 2017; revised July 31, 2017 and September 20, 2017; accepted October 10, 2017. This work was supported by the Government through DoD, Air Force Office of Scientific Research, National Defense Science and Engineering Graduate Fellowship under Grant 32 CFR 168a. This paper was recommended by Associate Editor Y. Sun. *(Corresponding author: Mark D. Hickle.)*

M. D. Hickle was with the School of Electrical and Computer Engineering and with the Birck Nanotechnology Center, Purdue University, West Lafayette, IN 47907 USA. He is now with BAE Systems, Inc., Merrimack, NH 03054 USA (e-mail: markhickle@ieee.org).

D. Peroulis is with the School of Electrical and Computer Engineering and also with the Birck Nanotechnology Center, Purdue University, West Lafayette, IN 47907 USA (e-mail: dperouli@purdue.edu).

Color versions of one or more of the figures in this paper are available online at http://ieeexplore.ieee.org.

Digital Object Identifier 10.1109/TCSI.2017.2766206

such as microstrip [14], [15], lumped elements [16], [17], and evanescent-mode cavities [18]–[21]. Despite the many excellent examples of absorptive bandstop filters which have been published, several aspects of this class of filter have not yet been investigated. For example, none of the aforementioned papers have discussed how to predict or optimize the tuning range over which a tunable absorptive bandstop filter can achieve very large stopband attenuation. Additionally, there has been no discussion of how to design an absorptive bandstop filter to meet a certain bandwidth requirement, no analysis of the design tradeoffs which must be made when designing such filters, and no step-by-step design procedure other than an iterative manual optimization process.

In response to these and other knowledge gaps, this paper seeks to present a detailed analysis of absorptive bandstop filters which furthers knowledge of this class of filter. A theoretical foundation for optimizing the tuning range over which absorptive bandstop filters can achieve (ideally) infinite attenuation is developed, along with design principles to increase their robustness to process variations. The tradeoffs between selectivity and tuning range, and the impact of non-ideal effects such as coupling dispersion, transmission-line length variation, and parasitic coupling are examined and design principles are developed to mitigate these effects.

First, the topology of an absorptive bandstop filter is presented, and relevant equations are derived in detail. The tradeoffs between various performance metrics such as bandwidth, tuning range, and sensitivity are examined, and practical design considerations are presented. A comparison of the relative benefits and drawbacks of higher-order versus lower-order filters is made. Lastly, a step-by-step design procedure is presented, and several varactor-tuned microstrip absorptive bandstop filters are designed, fabricated, and measured to validate the theory and design principles presented in this paper.

II. Design Principles of Absorptive Filters

A. Analysis of a Two-Pole Absorptive Bandstop Filter

A schematic representation of a two-pole absorptive bandstop filter is shown in Fig. 1(a). This circuit was first disclosed in [12] and [13], and the following analysis in Section II.A bears similarities to that in [12] and [14] but is included here for the completeness of this paper and to introduce the different notation and terminology used in this paper.

The filter consists of two resonators (represented as the solid circles labeled "1" and "2" in Fig. 1) coupled to a source-to-load transmission line of length θ with coupling coefficients $k_{E1,2}$, and coupled to each other with coupling coefficient k_{12}. Though represented as shunt-parallel RLC resonators in Fig. 1(b), the resonators can be implemented as any resonators which have parallel-RLC equivalent circuits near resonance. The coupling elements are implemented as admittance inverters whose characteristic admittances (3)-(4) are equal to their respective coupling values scaled by the resonator and system characteristic impedances as defined in [22]. With the sign convention used in this analysis, positive coupling provides a $+90°$ insertion phase whereas negative coupling yields a $-90°$ insertion phase. The source-to-load coupling is assumed to be an ideal TEM transmission line. The source and load, represented in Fig. 1 as hollow circles labeled "S" and "L", have impedances which are assumed in this analysis to be identical to the characteristic impedance of the transmission line. The expressions in Fig. 1 are defined as follows:

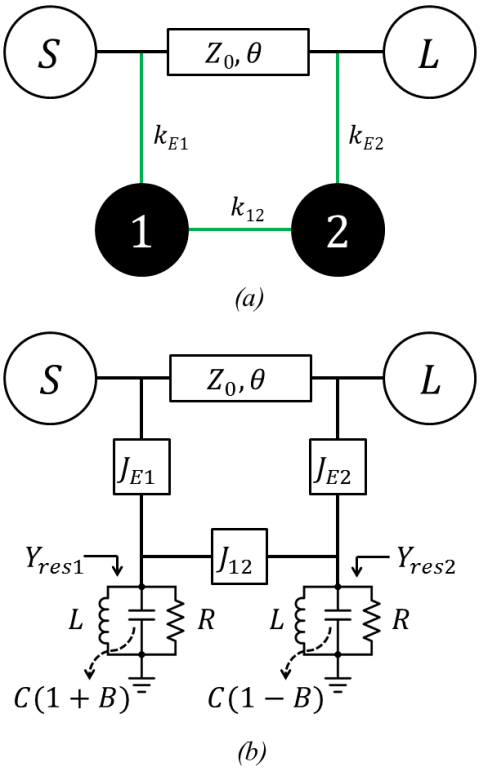

Fig. 1. (a) Schematic representation of a two-pole absorptive bandstop filter. (b) Equivalent circuit of (a). Source-to-load coupling is implemented by a transmission line of characteristic impedance Z_0 and electrical length θ, coupling elements are implemented by admittance inverters, and resonators are represented as parallel RLC resonators.

$$Y_{res1,2} = \frac{1}{Z_R}\left(\frac{1}{Q_U} + p \pm jB\right) \tag{1}$$

$$p = j\left(\frac{\omega}{\omega_0} - \frac{\omega_0}{\omega}\right) \tag{2}$$

$$J_{12} = k_{12}/Z_R \tag{3}$$

$$J_{E1,2} = k_{E1,2}/\sqrt{Z_0 Z_R} \tag{4}$$

$$Z_R = \sqrt{L/C} \tag{5}$$

$$\omega_0 = 1/\sqrt{LC} \tag{6}$$

$$Q_U = \frac{R}{\omega_0 L} = \omega_0 RC \tag{7}$$

$Y_{res1,2}$ represents the admittance of each resonator, and is simply the parallel combination of the admittances of the inductor, capacitor, and resistor which comprise each resonator, slightly rearranged and reduced using the definitions for the bandstop frequency variable (2), the resonators' impedances (5), and the resonators' unloaded quality factors (7). The capacitors are differentially tuned by a factor of $1 \pm B$, which allows for asynchronous tuning of the resonators if B is chosen

to be nonzero. The frequency-invariant reactance B in equation (1) which appears as a result of this differential capacitance tuning is only approximate – in reality the reactance would have frequency dependence, but in the narrowband case it can be approximated as constant. Equations (2) and (5-7) are derived from [23].

To obtain the transmission and reflection coefficients (S_{21} and S_{11}) of the circuit in Fig. 1(b), first the elements in the bottom branch of the circuit (the resonators and coupling elements) are cascaded together by multiplying their ABCD matrices. The resulting matrix is converted into its equivalent Y-parameter matrix [24], which is then added to the Y-parameter matrix of the transmission line due to their parallel configuration. The resulting Y-parameter matrix is converted into its equivalent S-Parameter matrix [24]. The resulting transmission and reflection coefficients are given in (8)–(10), as shown at the bottom of this page. Inspection of (8) shows that $S_{21} = 0$ at the filter's center frequency ($\omega = \omega_0$, or alternatively $p = 0$) when

$$\frac{1}{Q_U^2} + B^2 + k_{12}^2 + k_{12}k_{E1}k_{E2}\sin\theta = 0. \tag{11}$$

The filter has theoretically infinite attenuation even with finite-Q_U resonators if this equation is satisfied, and thus it is the governing equation for absorptive bandstop filters. The mechanism by which absorptive bandstop filters achieve infinite attenuation can be seen by examining the poles and zeros of S_{21}. For simplicity, the highpass prototype equivalent of (8) is used, which can be obtained by redefining (2) as $p = j\omega$. Equations for the poles and zeros can be found in [14]. Fig. 2(a) shows the poles and zeros of both a two-pole reflective bandstop filter and a two-pole absorptive bandstop filter. The reflective filter has a double zero which is offset from the $j\omega$ axis due to the use of finite-Q_U resonators, and thus has limited attenuation. The absorptive filter's interresonator coupling, along with the asynchronous tuning of its resonators, splits the zeros, restoring one zero to the origin while moving the other zero to the left in the complex plane. Thus the absorptive filter has infinite attenuation at its center frequency, but has less selectivity than a lossless two-pole bandstop filter which has two zeros at the origin. When $B = 0$, $k_{12} = 1/Q_U$, and $\theta = 90°$, as in the case of the perfectly-matched absorptive filter, the two poles fall on top of one of the zeros. This cancels a pole/zero pair, leaving one pole and one zero – corresponding to a lossless 1st order bandstop filter.

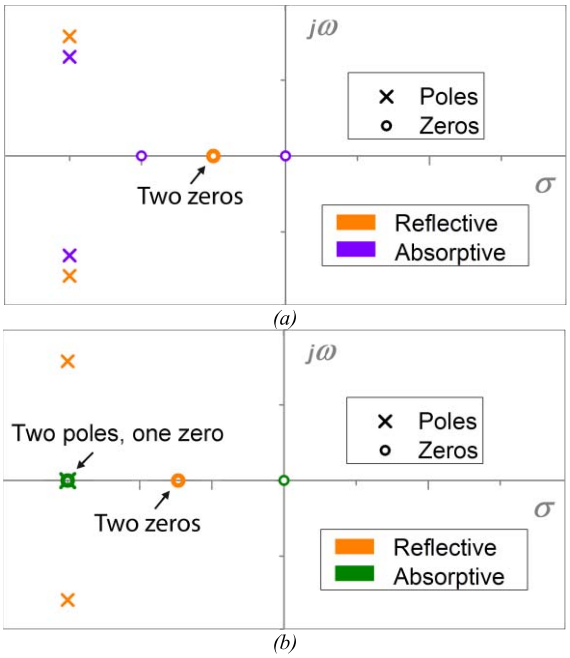

Fig. 2. Poles and zeros of S_{21} for (a) Reflective and absorptive bandstop filters, and (b) Reflective and perfectly-matched absorptive bandstop filters. In the case of the perfectly-matched absorptive bandstop filter, a pole and a zero cancel each other out, leaving a single pole/zero pair which corresponds to an ideal 1st order bandstop filter.

Many combinations of $k_{E1,2}$, k_{12}, B, Q_U and θ can provide valid solutions to (11), and thus it is instructive to examine the bounds placed on each variable, and to see how the choice of each variable affects the filter's transfer function. It should be noted that in the following analysis, the coupling coefficients ($k_{E1,2}, k_{12}$) and quality factor (Q_U) are assumed to be frequency-independent, and the transmission line length (θ) is assumed to be linearly proportional to frequency. While this is not precisely true in practice, this simplification is often sufficiently accurate in narrowband designs and is an important analysis step. Fine tuning and frequency-dependent effects are analyzed in Section III.

B. Limits on External Coupling

The limits on external coupling (k_{E1} and k_{E2}) can be found by solving (11) for k_{E1} and k_{E2}, which yields the

$$S_{21} = \frac{e^{-j\theta}\left(p^2 + \frac{2}{Q}p + B^2 + k_{12}^2 + \frac{1}{Q_U^2} + k_{12}k_{E1}k_{E2}\sin\theta\right)}{p^2 + \frac{4+(k_{E1}^2+k_{E2}^2)Q_U}{2Q_U}p + je^{-j\theta}k_{E1}k_{E2}(k_{12} + \frac{1}{2}k_{E1}k_{E2}\sin(\theta)) + \frac{1}{Q_U^2} + \frac{1}{2Q_U}\left(k_{E1}^2 + k_{E2}^2\right) + B^2 + k_{12}^2 + j\frac{B}{2}(k_{E1}^2 - k_{E2}^2)} \tag{8}$$

$$S_{11} = \frac{-\frac{1}{2}\left(k_{E1}^2 + e^{-2j\theta}k_{E2}^2\right)p + \mu}{p^2 + \frac{4+(k_{E1}^2+k_{E2}^2)Q_U}{2Q_U}p + je^{-j\theta}k_{E1}k_{E2}(k_{12} + \frac{1}{2}k_{E1}k_{E2}\sin(\theta)) + \frac{1}{Q_U^2} + \frac{1}{2Q_U}\left(k_{E1}^2 + k_{E2}^2\right) + B^2 + k_{12}^2 + j\frac{B}{2}(k_{E1}^2 - k_{E2}^2)} \tag{9}$$

$$\mu = -je^{-j\theta}k_{12}k_{E1}k_{E2} + \frac{e^{-2j\theta}k_{E2}^2\left(-2 + 2jBQ + k_{E1}^2Q\right)}{4Q} - \frac{k_{E1}^2(2 + 2jBQ + k_{E2}^2Q)}{4Q} \tag{10}$$

following equation:

$$k_{E1}k_{E2} = -\frac{\frac{1}{Q_U^2} + B^2 + k_{12}^2}{k_{12}\sin\theta} \tag{12}$$

This equation is similar to equation (8) in [12], with the important exception that it allows k_{E1} and k_{E2} to be different, both in magnitude and in sign. This provides two very useful insights about absorptive bandstop filters. First, it shows that the filter can still achieve infinite attenuation even with small variations in external coupling due to manufacturing variations as long as (12) can still be satisfied. Second, it shows that the relative polarities of k_{E1}, k_{E2}, and k_{12} dictate the length of transmission line which must be used.

For the signs of both the left- and right-hand sides of (12) to be consistent, the sign of the quantity $k_{E1}k_{E2}k_{12}sin\theta$ must be negative. Therefore if either one or three of the variables k_{E1}, k_{E2}, and k_{12} are negative, then sin θ must be positive ($0° < \theta < 180°$. However, if all of the aforementioned variables are positive, or two of them are negative, then sin θ must be negative ($180^o < \theta < 360^o$). This is a key fact because as shown in Section II.D, the length of source-to-load transmission line is critical when maximizing the tuning range of the filter.

Though they can differ in sign as dictated by the physical coupling structure, the magnitudes of k_{E1} and k_{E2} are usually chosen to be equal for the sake of simplicity (i.e. $k_{E1} = k_E = \pm k_{E2}$). For a given k_{12}, Q_U, and θ, the minimum k_E which will allow ideally infinite attenuation is

$$k_{E,min} = \sqrt{\frac{\frac{1}{Q_U^2} + k_{12}^2}{k_{12}\sin\theta}}, \tag{13}$$

which occurs when $B = 0$. For any value of k_E larger than (13), B can be chosen by asynchronously tuning the resonators such that (12) is still satisfied. Minimizing (13) with respect to k_{12} and θ shows that the absolute minimum possible value for k_E for a given Q_U is

$$k_{E,min}^* = \sqrt{2/Q_U}, \tag{14}$$

obtained when $k_{12} = 1/Q_U$, and $\theta = 90°$. If these values are substituted into (9), it can be seen that the filter has zero reflection coefficient, and thus is a perfectly-matched absorptive bandstop filter [12]. When k_E is larger than this absolute minimum value, the reflection coefficient is nonzero, and increases with increasing k_E as shown in Fig. 3.

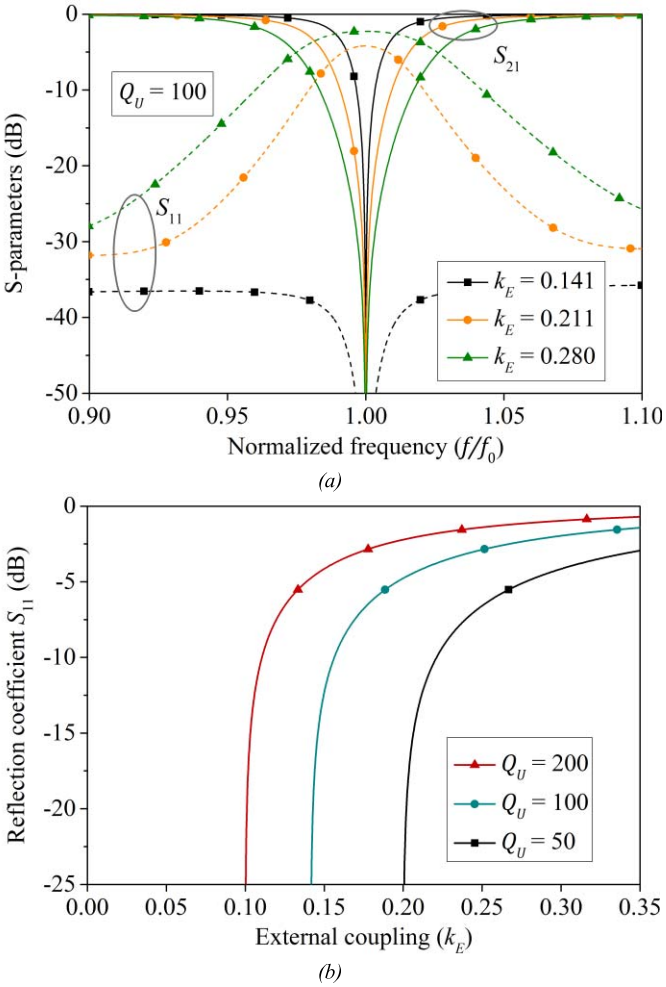

Fig. 3. (a) The effect that k_E has on bandwidth and reflection coefficient. (b) Variation of maximum reflection coefficient (at $\omega = \omega_0$) with k_E. $k_{12} = 1/Q_U$ and $\theta = 90°$ in both figures. At the minimum value of k_E ($\sqrt{2/Q_U}$), the filter is perfectly matched and has zero reflection coefficient. When k_E is increased beyond its minimum value, the reflection coefficient becomes nonzero and increases with k_E. In each case the filter has infinite attenuation at its center frequency.

C. Limits on Interresonator Coupling

Solving (11) for k_{12} yields the following equation:

$$|k_{12}| = \frac{1}{2}\left[k_E^2|\sin\theta| \pm \sqrt{(k_E^2\sin\theta)^2 - \frac{4}{Q_U^2} - 4B^2}\right] \tag{15}$$

All solutions for k_{12} come in pairs due to the quadratic nature of the equation. When $B = 0$, the two solutions represent the maximum and minimum allowable values of k_{12} for given k_E, Q_U, and θ. For all values of k_{12} between these extrema, B can be chosen by asynchronously tuning the resonators such that (15) is satisfied. Fig. 4 shows the maximum and minimum allowable values for k_{12} plotted versus k_E, for several values of Q_U. Note that when k_E is equal to its minimum value (14), there is only one possible value for k_{12}, whereas for k_E greater than (14) a range of values of k_{12} are possible. This is an important fact for designs which are robust to process variations. If the minimum k_E is chosen, then any slight variation in Q_U, k_{12}, or k_E will not allow infinite attenuation. This can make the design process particularly challenging, because it is often difficult to accurately predict the unloaded qualify factor of tunable resonators. By choosing k_E larger than its minimum value, however, the design is desensitized to process variations, and small variations in k_E, Q_U, or k_{12} can be compensated by asynchronously tuning the resonators. However, this comes at the expense of decreased selectivity as is seen in Section II.E.

The ability to compensate for variations in k_E, k_{12}, Q_U, and θ by asynchronously tuning the resonators has previously been noted in [12]. However, this analysis shows for the first time the range of values of k_E and k_{12} that can be compensated

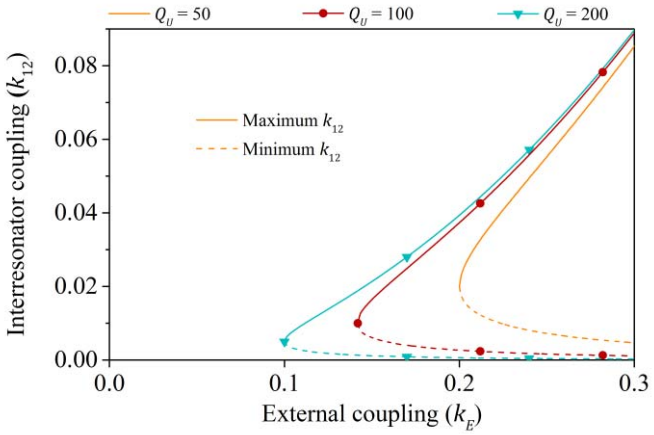

Fig. 4. Maximum and minimum allowable values for interresonator coupling (k_{12}) plotted versus external coupling (k_E) and unloaded quality factor (Q_U), obtained from (15) with $B = 0$. At the minimum value of k_E ($\sqrt{2/Q_U}$), there is only one permissible value for k_{12} ($1/Q_U$). A broader range of values for k_{12} can be used when k_E is increased beyond its minimum value, providing design flexibility and decreased sensitivity to process variations.

by asynchronous tuning, and that the design robustness can be increased by increasing the value of k_E

D. Tuning Range

Since (11) depends on the electrical length of the through-line (θ), which is proportional to frequency, it can only have solutions for a certain range of frequencies. Solving (11) for θ with $B = 0$ yields the minimum and maximum allowable values of θ for a given Q_U, k_{12}, k_{E1}, and k_{E2}:

$$\theta_{min} = \sin^{-1}\left(\frac{\frac{1}{Q_U^2} + B^2 + k_{12}^2}{k_E^2 k_{12}}\right) + n180° \tag{16}$$

$$\theta_{max} = 180° - \theta_1 + n360° \tag{17}$$

where n is an even integer if the sign of $k_{E1}k_{E2}k_{12}$ is negative, and an odd integer if the sign of $k_{E1}k_{E2}k_{12}$ is negative.

With an ideal, dispersionless transmission line, the electrical length (θ) of the transmission line is linearly proportional to frequency. The ratio of $\theta_{max}/\theta_{min}$ is equivalent to the ratio f_{max}/f_{min}, and this ratio can tell us the tuning range of the filter – that is, the range of center frequencies for which (11) can be satisfied. This ratio, designated as the tuning range (TR), is

$$TR = \frac{\theta_{max}}{\theta_{min}}. \tag{18}$$

If one seeks to design a widely-tunable absorptive bandstop filter, it is desirable to know how the choice of design parameters affects the tuning range, and how to increase the tuning range. The tuning range increases monotonically with Q_U and k_E, as shown in Fig. 5. However, it can be shown that there is an optimal value for k_{12} which maximizes (18):

$$k_{12,opt} = 1/Q_U \tag{19}$$

This optimal value of k_{12} can be seen in Fig. 6, which plots tuning range as a function of k_{12} for different values of k_E. It should be noted that this is the same value of k_{12} which minimizes k_E, as in equation (13).

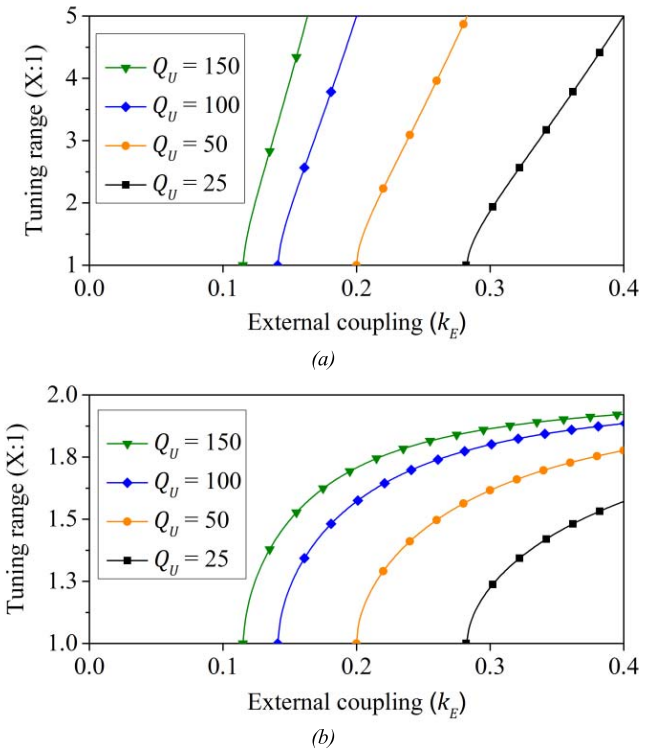

Fig. 5. Tuning range plotted versus external coupling with (a) a nominally 90° and (b) a nominally 270° source-to-load transmission line. Interresonator coupling k_{12} is the $1/Q_U$.

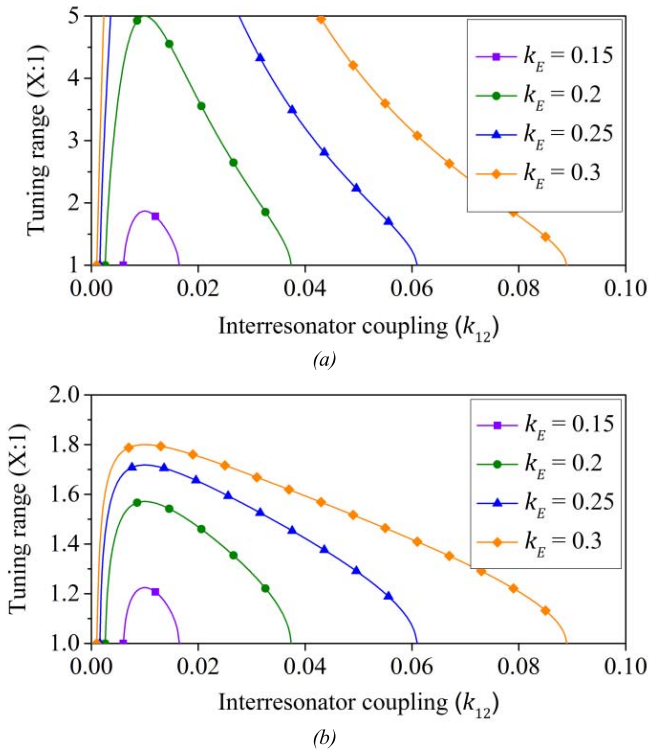

Fig. 6. Tuning range plotted versus interresonator coupling with (a) a nominally 90° and (b) a nomninally 270° source-to-load transmission line. $Q_U = 100$.

By observing the limits on the numerator and denominator of (18), the absolute maximum tuning range can be determined. If k_E is chosen arbitrarily large and

a nominally 90° line is used, then it can be seen that $\theta_{\max}$ approaches 180° and $\theta_{\min}$ approaches 0°. The maximum tuning range is then $180^o/0^o$ or $\infty : 1$, indicating that if k_E is chosen to be large enough an arbitrarily large tuning range can be achieved. In practice however, the tuning range is limited by how large k_E can practically be realized. If the nominal θ is 270°, then as k_E becomes infinitely large, $\theta_{\max}$ approaches 360° and $\theta_{\min}$ approaches 180°. The ideally maximum tuning range is then 360°/180°, or 2:1. This shows that the maximum possible tuning range for a filter with a nominally 270° through line is one octave, although in practice the finite physically-realizable values of k_E will result in less than a 2:1 tuning range. Though a filter with a 90° line cannot provide an infinite tuning range when practical coupling values are considered, it will always provide a larger tuning range than a filter utilizing a 270° through-line for a given k_E, Q_U, and k_{12}. The same procedure shows that further increasing lengths of transmission line result in further decreasing tuning ranges. It is clear that if a wide tuning range is desired, the length of through-line should be chosen as short as possible. A 90° through line is always preferable from this perspective, but in practice it is not always possible. As explained in Section II.A, the required length of transmission line depends on the relative signs of the coupling elements, and some filter technologies have no flexibility in the sign of the coupling elements or must sacrifice complexity or performance in order to change the coupling sign. In other situations, particularly at high frequencies and in designs on high-permittivity substrates, a 90° transmission line might be too short to practically implement between the resonators. Thus, it is necessary to investigate the performance of absorptive filters which utilize nominally 270° through-lines.

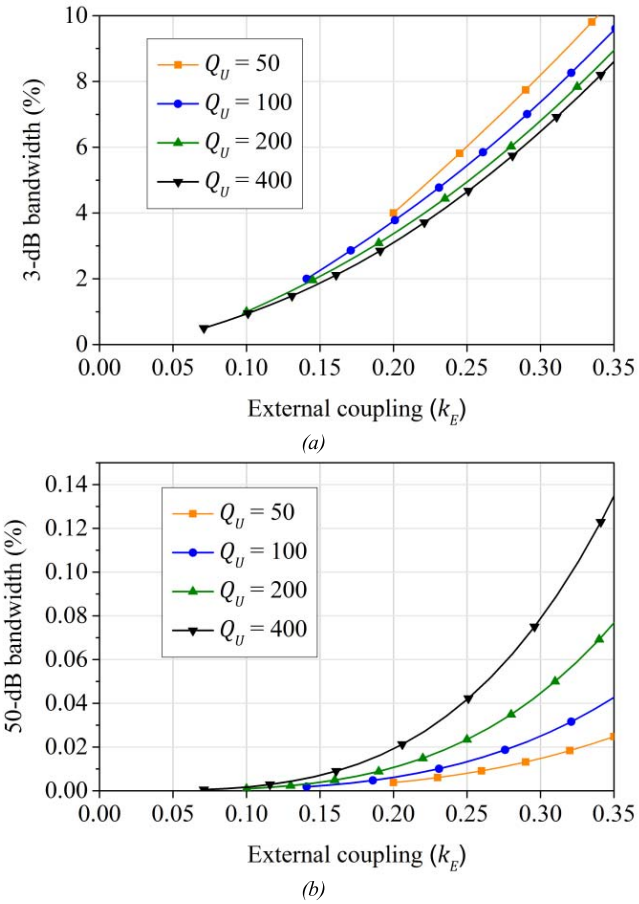

Fig. 7. Dependence of (a) 3-dB and (b) 50-dB fractional bandwidths on external coupling and unloaded quality factor.

E. Bandwidth

Bandwidth is a critical design parameter of bandstop filters, and thus it is important to determine the dependence of bandwidth on the various filter design variables. The X-dB bandwidth of the filter (defined as the bandwidth of the filter at an attenuation level of X dB) can be obtained from (8):

$$BW = \sqrt{\frac{1}{R}\left[L_A\,(2+K) - 2 + \frac{1}{2}\sqrt{16+Z}\right]} \tag{20}$$

$$Z = \left(K^2-4\right)\left[4\,(2-L_A) + K\,(4+K)\,(1-L_A)\right]L_A \tag{21}$$

$$R = Q_U^2\,(1-L_A) \tag{22}$$

$$K = k_E^2 Q_U \tag{23}$$

$$L_A = 10^{-\frac{X}{10}} \tag{24}$$

The transmission line length θ is set equal to 90° in order to simplify the equations. If $k_E = \sqrt{2/Q_U}$, as in the case of a perfectly-matched absorptive bandstop filter as described in Section II.B, then equation (20) reduces to

$$BW = 2/(Q_u\sqrt{10^{\frac{X}{10}}-1}) \tag{25}$$

which identical to the equation for the bandwidth of absorptive bandstop filters derived in [12].

The dependence of 3-dB and 50-dB bandwidths on k_E and Q_U are shown in Fig. 7. The bandwidth has a strong dependence on k_E, and a weaker dependence on Q_U. Although high levels of attenuation can be achieved regardless of resonator quality factor, higher selectivity (narrower 3-dB bandwidth and larger 50-dB bandwidth) can be achieved with higher-Q_U resonators.

The dependence of 3-dB bandwidth on the length of the through-line (θ) can be obtained through simulation, and is shown in Fig. 8. For a nominally 90° through-line, the bandwidth variation with respect to θ is minimal for realistic values of θ which will be encountered in a tunable filter. However, when a nominally 270° through-line is used, even a filter with a tuning range of 1.5:1 can experience bandwidth variations of 20% or more. The choice of k_{12} has very little effect on bandwidth, as long as it is chosen according to (15).

Because the tuning range and the bandwidth are both strongly dependent on k_E, it is possible to examine the maximum tuning range for a given bandwidth, and vice versa. A plot of bandwidth vs. tuning range for several values of Q_U is shown in Fig. 9. From this graph it can be seen that in order to increase tuning range by increasing k_E, the bandwidth must also be increased. However, if higher Q_U resonators can be used, the same tuning range can be obtained with a smaller bandwidth. This effect is much more prominent for filters with

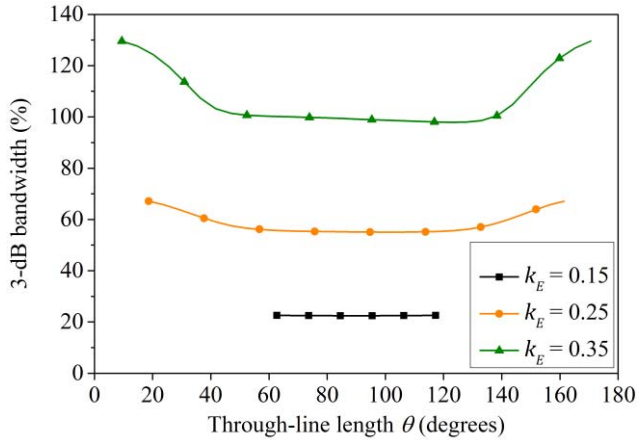

Fig. 8. Effect of through-line length (θ) on 3-dB bandwidth. $Q_U = 100$, $k_{12} = 0.01$.

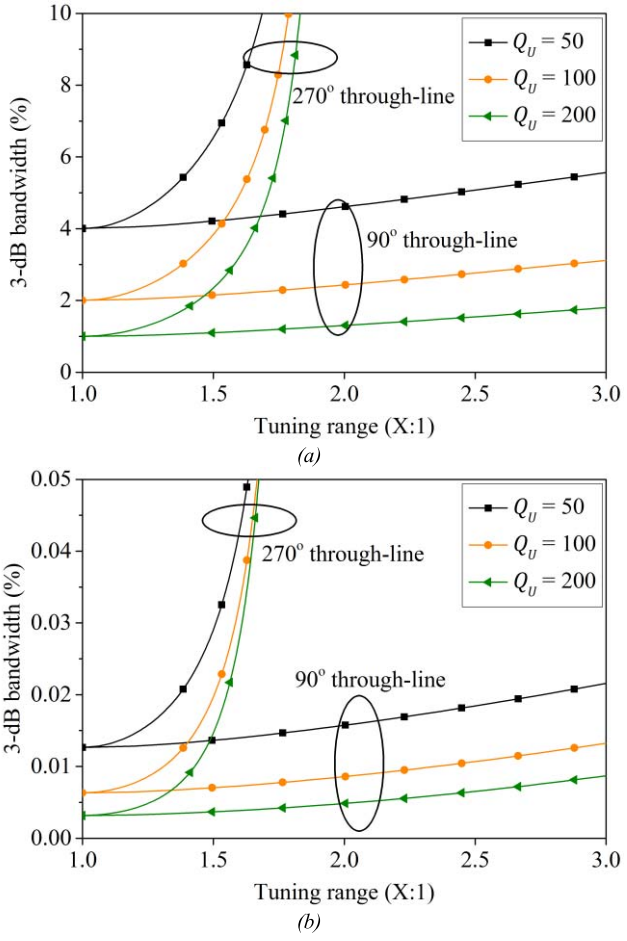

Fig. 9. Relationship between tuning range and minimum (a) 3-dB and (b) 50-dB fractional bandwidths. Larger tuning ranges require larger values of k_E, which results in wider bandwidths. $|k_{12}| = 1/Q_U$.

nominally 270° through-lines, which are limited to a maximum possible tuning range of 2:1.

F. Higher Order Filters

Although a two-pole absorptive bandstop filter is able to achieve large maximum attenuation, it can only do so over a very narrow bandwidth. For example, the two-pole

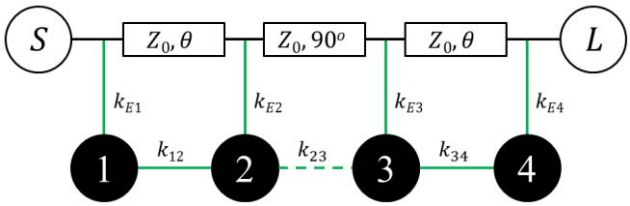

Fig. 10. Schematic of a four-pole absorptive filter created by cascading two two-pole sections with a 90° transmission line between sections. Undesired inter-stage coupling is represented with the dashed line (k_{23}).

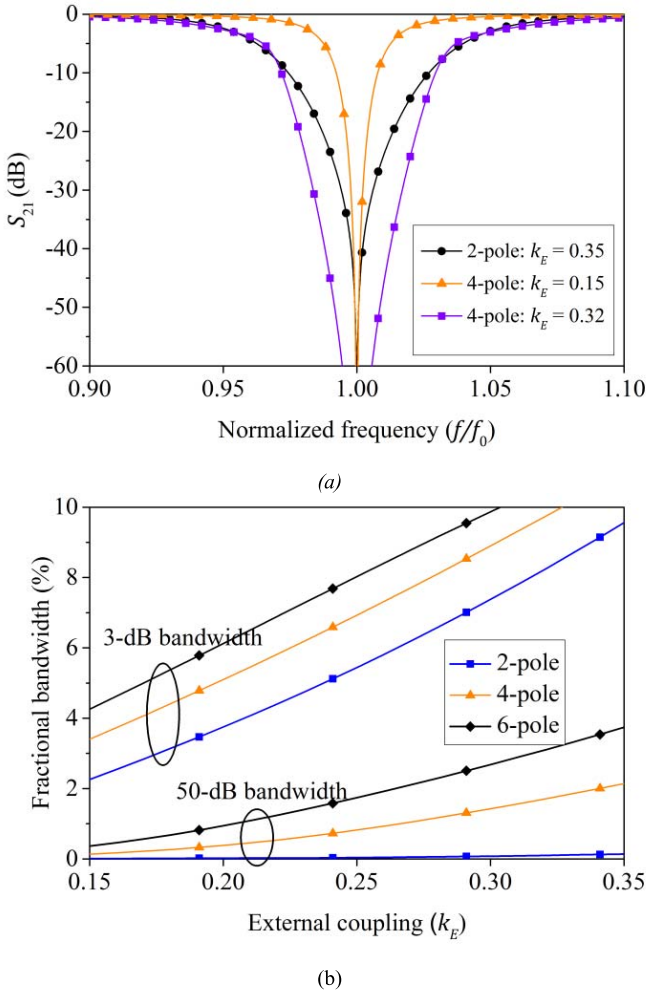

Fig. 11. (a) Comparison of 2-pole filter response with 4-pole response which have equal 3-dB bandwidth (purple trace) and equal 40-dB bandwidth (orange trace). (b) Comparison of bandwidths for 2-pole, 4-pole, and 6-pole filters. $Q_U = 100$, $\theta = 90°$, and $k_{12} = 1/Q_U$ in both graphs.

filter in Fig. 11(a) only has a 0.14% 50-dB bandwidth for a 3-dB bandwidth of 9.7%. If high attenuation is required over a wider bandwidth, the order of the filter can be increased by cascading two or more two-pole stages. In general 90° transmission lines are required in order to have a symmetric filter transfer function [25], due to the impedance mismatch between the stages. However, in cases where the two-pole stages have very small reflection coefficients (as discussed in Section II.B), the impedance mismatch between stages is less pronounced and the exact length of the inter-stage

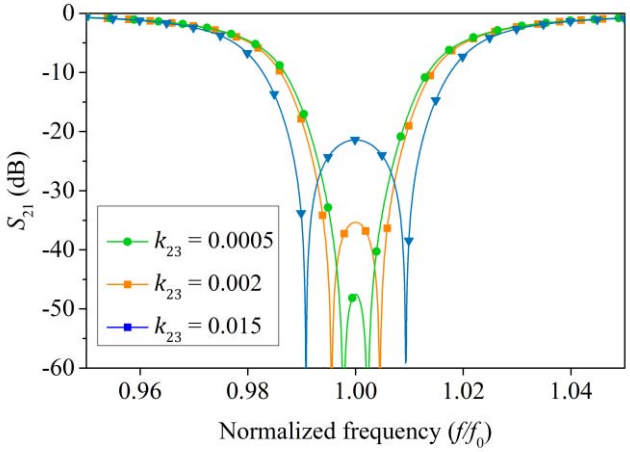

Fig. 12. Effect of parasitic inter-stage coupling (k_{23}) on filter performance. Even very small amounts of parasitic coupling can degrade filter performance by limiting the maximum achievable equiripple attenuation level.

transmission line becomes less important. For example, in [14] and [15], approximately 30° long inter-stage transmission lines are used. The increased selectivity of higher-order filters is shown in Fig. 11(a), in which the four-pole filter (purple trace) has a 12× greater 50-dB bandwidth (1.7%) than the two-pole filter, for the same 3-dB bandwidth. This comes at the expense of a smaller tuning range and increased passband insertion loss, however. It can be seen in Fig. 11(b) that four- and six-pole filters require smaller external coupling (k_E) values than a two-pole filter for an equivalent 3-dB bandwidth, and this reduces the center-frequency tuning range over which the filter can achieve high attenuation as discussed in Section II.D.

It is critical to prevent coupling between the stages when cascading 2-pole stages to form higher-order filters. Parasitic coupling between the two adjacent resonators of the separate stages (k_{23} in Fig. 10) reduces the maximum level of attenuation by a pole-splitting effect. Fig. 12 shows the maximum attenuation states of a four-pole filter with various levels of parasitic inter-stage coupling.

III. Design of Microstrip Absorptive Bandstop Filters

To verify the preceding design principles and demonstrate a practical design example, four microstrip-based absorptive bandstop filters were designed. All filters were implemented with varactor-tuned, grounded quarter-wave microstrip resonators, chosen for their ease of implementation, ability to achieve wide tuning range, compact size, and wide spurious-free response. All filters were designed to operate over a 1.25 to 2.5 GHz tuning range. Filters A and B were designed to demonstrate that the required length of source-to-load through-line depends on the sign of the couplings as stated in Section II.B, and that using a nominally 90° through-line results in a wider tuning range than using a nominally 270° through-line. Filter A utilizes positive mutual inductance as interresonator coupling, which provides +90° insertion phase and thus requires a nominally 270° through-line. Filter B reverses the sign of interresonator coupling by reversing the

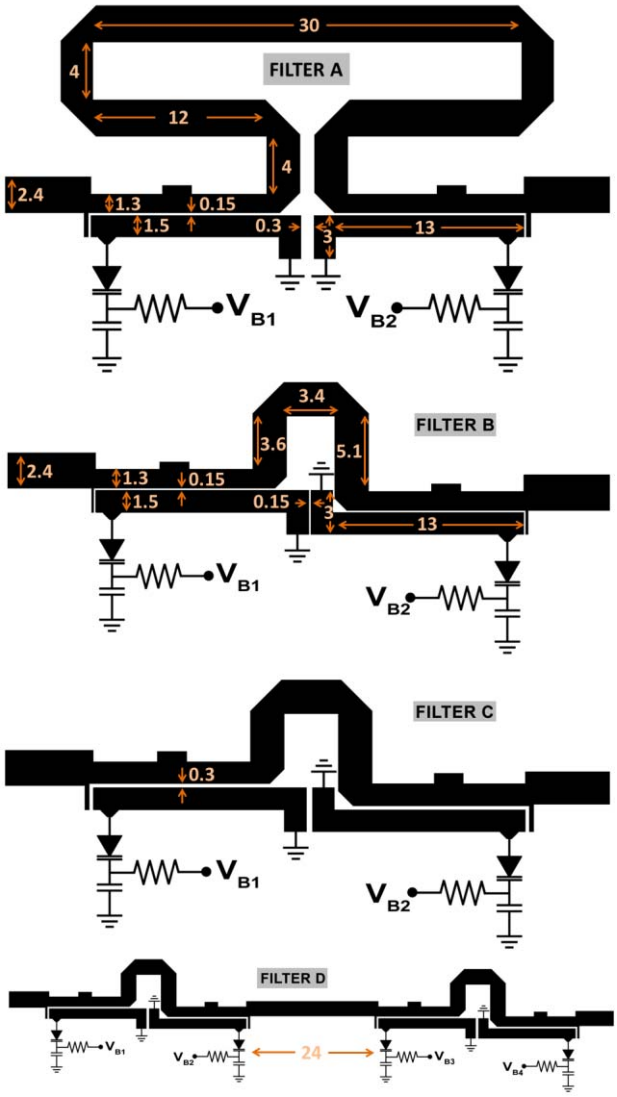

Fig. 13. Layout and dimensions of the designed filters. All dimensions are in millimeters. VB1,2,3,4 denote the varactors' bias voltages.

position of the grounding via, and thus requires a nominally 90° through-line. The 3-dB bandwidths of Filter A and Filter B are equal: 5% at 1.5 GHz. Filter C utilizes a 90° through-line and is identical to Filter B with the exception of a narrower 3-dB bandwidth: 2.5% at 1.5 GHz. It illustrates the tradeoff between bandwidth and tuning range, as it has a narrower bandwidth and thus a smaller tuning range than the otherwise-identical Filter B. The fourth filter (Filter D) consists of two Filter Cs cascaded to form a four-pole filter, and illustrates increased selectivity with the penalty of reduced tuning range when compared to a 2-pole filter, as discussed in Section II.F. A detailed design procedure for Filter B is shown next. The design procedures for the other filters are omitted for brevity, but are essentially identical to the procedure used to design Filter B.

First, the varactors and the dimensions of the resonators were selected to yield the desired tuning range using a standard design procedure such as in [23]. MACOM MA46H202 GaAs hyperabrupt tuning varactors were chosen for their high Q_U

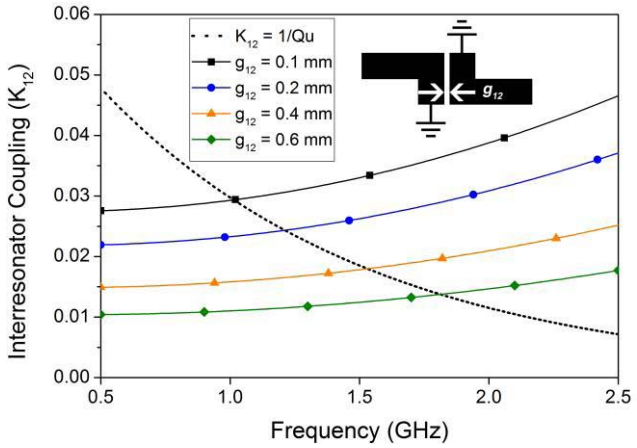

Fig. 14. Frequency dependence of interresonator coupling, extracted from electromagnetic simulations.

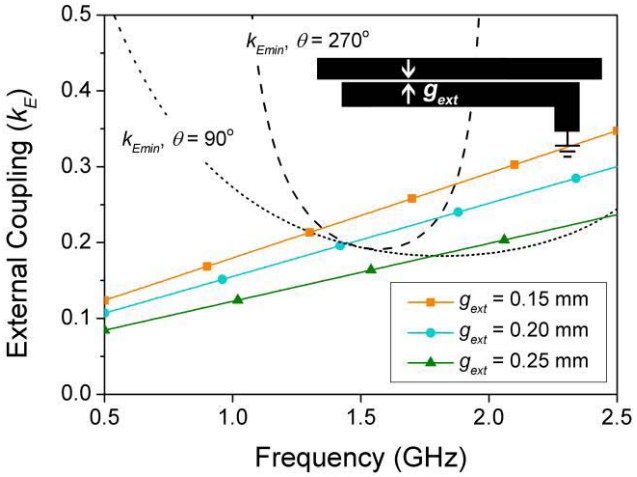

Fig. 15. Minimum required external coupling ($K_{E,min}$) and simulated external coupling values for different coupling gaps (g_{EXT}). For all frequencies where the actual value of K_E is greater than $K_{E,min}$ the filter can achieve an absorptive response $g_{12} = 0.15$ mm.

and wide tuning range (0.6-6pF, $Q_U = 2000$ at 50 MHz). Using the information in the varactor's datasheet and electromagnetic simulation of the microstrip resonators, the unloaded quality factor was estimated at different frequencies in order to aid in choosing the interresonator coupling coefficient.

Design curves for interresonator coupling (k_{12}) versus frequency for different resonator spacings were calculated from electromagnetic simulation according to the method in [26] and are plotted in Fig. 14. The optimal value of k_{12} ($1/Q_U$) which allows for the minimum value of k_E was calculated using the estimated values of Q_U, and is also plotted in Fig. 14. It decreases with increasing frequency because of the frequency dependence of the resonator's unloaded quality factor, and it is clear that it has the opposite trend as the actual values of k_{12} which increase with frequency. Because smaller values of Q_U and k_E increase the design's sensitivity to the choice of k_{12} (see (15) and Fig. 4), k_{12} should be chosen such that it is equal to its optimal value at the lowest frequency of the tuning range, where Q_U and k_E are the smallest. From the graphs in Fig. 14, the interresonator coupling gap g_{12} was initially chosen to be 0.25 mm in order to provide a coupling coefficient of 0.02 at 1.25 GHz, the optimal coupling coefficient for a resonator Q_U of 50. This serves as a starting point for fine tuning later in the design process.

The through transmission line length was initially chosen to be 29 mm long (90° long at 1.9 GHz, the mid-point of the filter's tuning range), measured from the outside extremities of the resonators. Choosing the through-line to be 90° at the center of the tuning range minimizes the deviation of its electrical length from a quarter wavelength, which is the required length of transmission line for a symmetric bandstop filter response [25]. This also serves as a starting point for fine tuning later in the design process.

Once the frequency-dependent values of Q_u and k_{12} are known and the transmission line length has been chosen, the minimum value of k_E required to obtain an absorptive response can be calculated from equation (13). Fig. 15 shows the minimum required values of k_E for nominally 90° (Filter B) and 270° (Filter A) through-lines, along with k_E extracted for several values of g_{ext}. The method in [27] is used to extract k_E from simulations. Due to the frequency-dependence of k_{12}, k_E, and Q_U, the equation developed for calculating the tuning range (18) cannot directly be used. However, from these design curves the tuning range can be determined by noting the frequency range for which the simulated value of k_E is greater than the minimum required value of k_E. It is evident that in all cases the tuning range for a nominally 90° through-line is greater than a nominally 270° line for an equal k_E value, and that increasing k_E increases the tuning range.

Finally, the interresonator coupling gap g_{12} and the length of the through transmission line were fine-tuned in order to maximize the filter's tuning range by maximizing the range over which k_E was greater than k_{Emin}. It was found that due to the strong frequency dependence of k_E, the low end of the filter's tuning range was limited due to low values of k_E and Q_U, whereas there was no limit on the high end of the filter's tuning range because both k_E and Q_U were both much larger at these frequencies. The transmission line length was increased to 38 mm to further improve the lower limit of the filter's tuning range, at the expense of slight asymmetry of the filter's transfer function at the upper end of its tuning range where the transmission line is significantly longer than the quarter wavelength required for a symmetric transfer function.

This design procedure is convenient in that it approaches the design of each design parameter individually, based on the design principles presented in this paper. Each of these parameters can be evaluated without performing EM simulations of the entire filter, and minimal fine-tuning of the entire circuit is required at the end of this process. This is in contrast to the design procedures presented in [14] and [15], which manually optimize the circuit without the guidance of clear design principles.

An alternative design procedure is to simply calculate the achievable tuning range for all practical values of g_{EXT} and g_{12}, and then choose combination that yields the desired tuning range. The tuning range of the filter can be determined by numerically calculating the range of frequencies for which

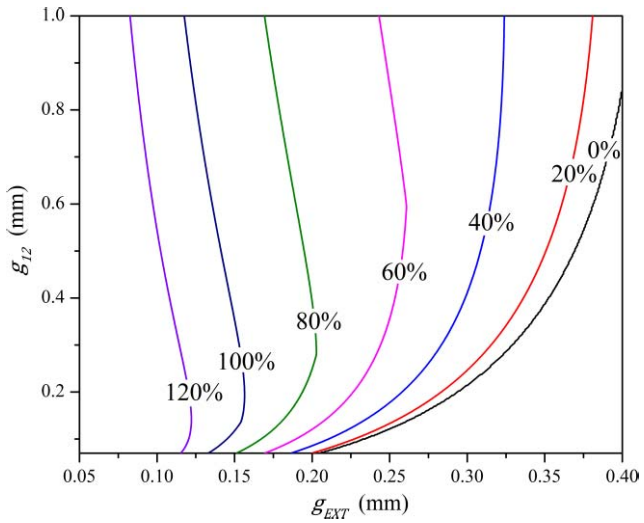

Fig. 16. Contour plot indicating the achievable tuning range of Filter B for various combinations of g_{EXT} and g_12.

the left-hand side of (11) is greater than zero. This can be done by utilizing the frequency-dependent values of Q_U, θ, and the k_E and k_{12} which result from a given combination of g_{EXT} and g_{12}. Though it is not practical to extract the frequency-dependent values of k_E and k_{12} for every value of g_{EXT} and g_{12}, one can extract the frequency-dependent coupling values for a few values of g_{EXT} and g_{12}, then interpolate between these points to obtain the rest of the values. Because k_E and k_{12} are well-behaved functions of g_{EXT} and g_{12}, it was found that extracting k_E and k_{12} for three to four values of g_{EXT} and g_{12} provided sufficient accuracy. Using this method, the contour plot in Fig. 16 indicating the achievable tuning range as a function of g_{EXT} and g_{12} was created. From this plot, it can be seen that larger tuning ranges require smaller values of g_{EXT}, which correspond to larger values of k_E. Also, the optimal value of g_{12} decreases as the tuning range increases, because the optimal k_{12} is approximately $1/Q_U$ at the lower end of the tuning range, and thus k_{12} increases as tuning range increases.

Using this design process, Filters A and B were designed with the same external coupling coefficient in order to have the same bandwidth ($g_{EXT} = 0.15$ mm in Fig. 15, for a 3-dB bandwidth of approximately 5% at 1.5 GHz) and Filters C and D were designed with a smaller external coupling coefficient for a narrower bandwidth ($g_{EXT} = 0.25$ mm in Fig. 15, for a fractional bandwidth of approximately 2.5% and 3.5%, respectively, at 1.5 GHz). The final dimensions of all filters are shown in Fig. 13.

The procedure for designing tunable absorptive bandstop filters with the minimum 3-dB bandwidth for a given tuning range can be summarized as follows:

1) Select resonators and tuning elements to cover desired frequency range, choosing a resonator topology for which the sign of $k_{E1}k_{E2}k_{12}$ is negative so that a 90° through-line can be used.
2) Extract k_{12}-versus-frequency and Q_U-versus-frequency curves, and choose $k_{12}$to be equal to $1/Q_U$ near the lower end of the desired tuning range.

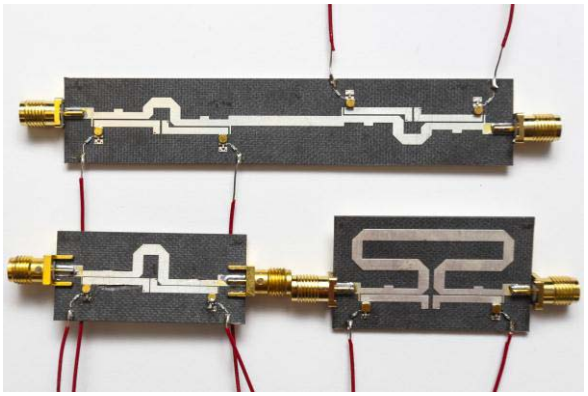

Fig. 17. Photograph of fabricated filters. Clockwise from top: Filter D, Filter A, and Filter B. Filter C is not shown because it is nearly visually indistinguishable from Filter B, as shown in Fig. 13.

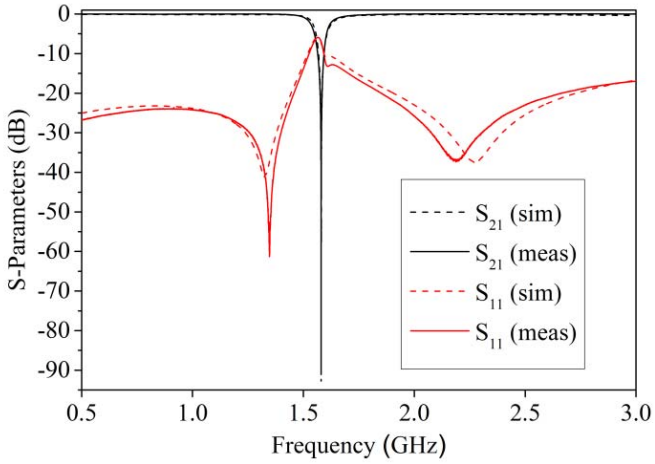

Fig. 18. Simulated and measured response of Filter B when tuned to 1.6 GHz.

3) Plot $k_{E,min}$ calculated from (13) using frequency-dependent values of Q_U and k_{12}, choosing the through-line to be 90° (or 270°, as dictated by the coupling signs) near the center of the desired tuning range.
4) Extract k_E-versus-frequency curves, and choose the lowest value of k_E which is larger than the $k_{E,min}$ curve over the desired frequency range.
5) If necessary, fine-tune k_{12} and θ in order to maximize the filter's tuning range by using simulated k_E and calculated $k_{E,min}$ curves, as in Fig. 15.

IV. Experimental Validation

The filters were fabricated on 0.787-mm thick Rogers RT/Duroid 5880 substrate ($\varepsilon_r = 2.2 \pm 0.02$, $\tan\delta = 0.0009$), and measured using a Keysight N5230C PNA. The varactors were biased between 4 and 22 V with a Keysight N6705B voltage source, using series 10 k Ω resistors to provide RF isolation between the resonator and the power supply, and shunt 56 pF capacitors to provide AC grounds for the varactors. A photograph of Filters A, B, and D is shown in Fig. 17. Fig. 18 shows the measured frequency response of Filter B tuned to 1.6 GHz, illustrating its high-attenuation stopband and well-matched, low-loss passband. It has less than 0.2 dB

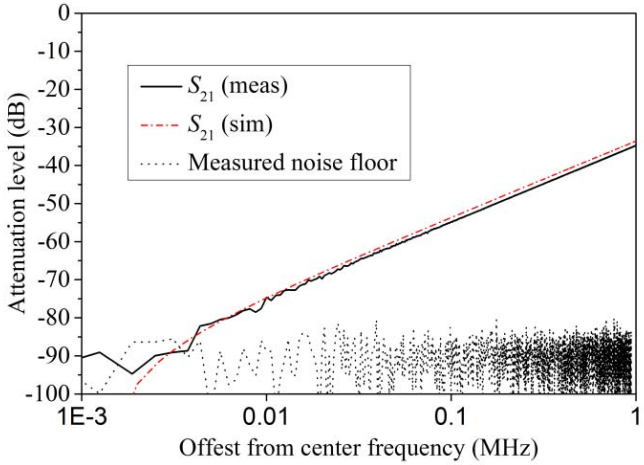

Fig. 19. Measured attenuation in stopband of filter.

passband insertion loss up to 3 GHz. As expected, the filter is able to achieve very high attenuation in its stopband (over 90 dB), although the bandwidth at high levels of attenuation is limited. Fig. 19 shows the measured attenuation plotted versus offset from the filter's center frequency. The filter has a 4.9% 3-dB bandwidth, 1.8% 10-dB bandwidth, 0.15% 30-dB bandwidth and 0.0015% 70-dB bandwidth. The measured attenuation is limited by the noise floor of the network analyzer, which is also plotted in Fig. 19.

In order to verify the design principles of Section II and the design procedure of Section III, the measured responses of each of the filters when tuned over their entire tuning ranges are shown in Fig. 20. As expected from the theory in Section II.D, Filter B has a wider tuning range than Filter A due to its use of a nominally 90° instead of 270° through-line (1.45:1 versus 1.27:1). Additionally, Filter B also has a wider tuning range than Filter C due to its larger bandwidth (1.45:1 versus 1.24:1). The high-attenuation tuning range of each filter is smaller than designed because the quality factors of the varactors used were much lower than specified in the datasheets. The extracted quality factor of the varactors varied from 34 to 87 between 1 and 2 GHz, compared to the Q_U of 77 to 220 specified in the datasheet. When the extracted value of varactor Q_U and the slight fabrication dimensional errors are taken into account, the measured results match simulation very well in Fig. 18.

The performance of the four-pole filter (Filter D) is compared to that of the wide-bandwidth two-pole filter (Filter B) in Fig. 21. The two filters have identical 10-dB bandwidths, but as expected the four-pole filter has greatly increased selectivity, with a 20× greater 50-dB bandwidth (9.84 MHz versus 492 kHz) and a 22% smaller 3-dB bandwidth (184 MHz versus 237 MHz). As seen in Fig. 20, however, the maximum attenuation of Filter D is maintained over a narrower tuning range than Filter B (1.9 to 2.3 GHz, as compared to 1.59 to 2.3 GHz) because a smaller value of k_E is needed to obtain the same 10-dB bandwidth. Additionally, Filter D had a higher level of passband insertion loss than did Filter B (0.55 dB compared to 0.2 dB at 3 GHz) due to the longer lengths of transmission lines used.

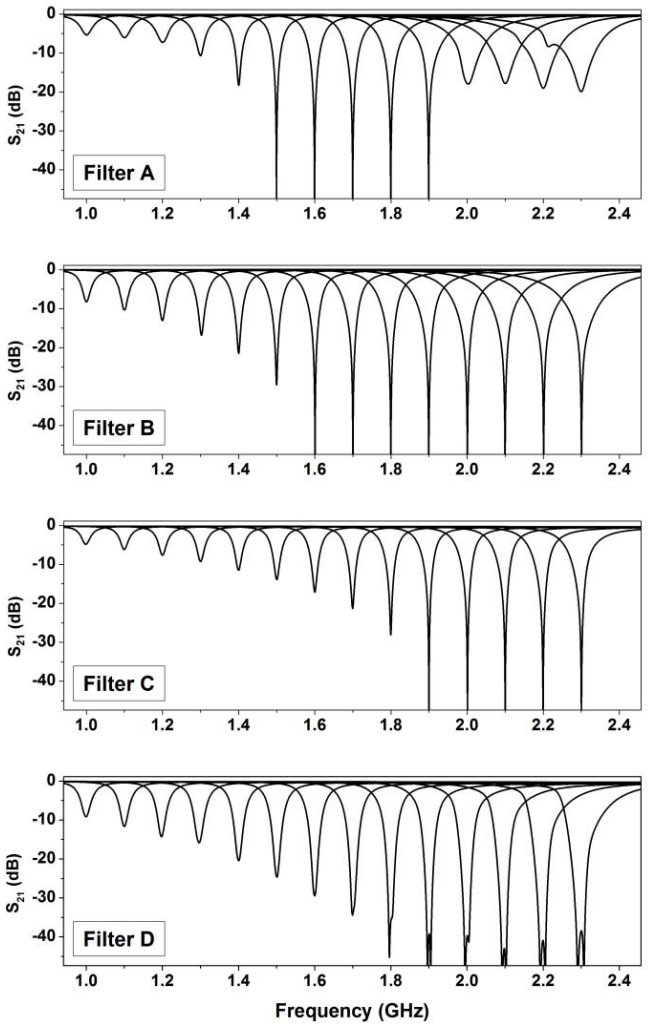

Fig. 20. Measured transmission responses of all filters tuned across their frequency ranges.

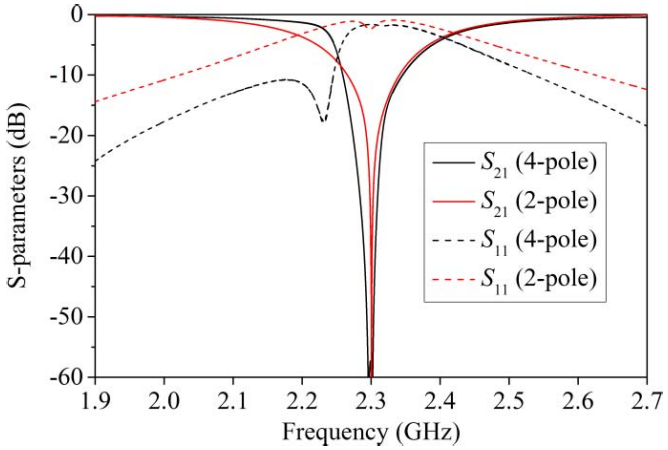

Fig. 21. Comparison of two- and four-pole filters. The four-pole filter exhibits greatly increased selectivity, but does not maintain high attenuation over as large of a frequency range as the two-pole filter.

The two-pole filter would be well-suited for applications in which a narrow bandwidth of high attenuation is needed, but over a wide tuning range. In contrast, the four-pole filter would be better-suited for applications in which high

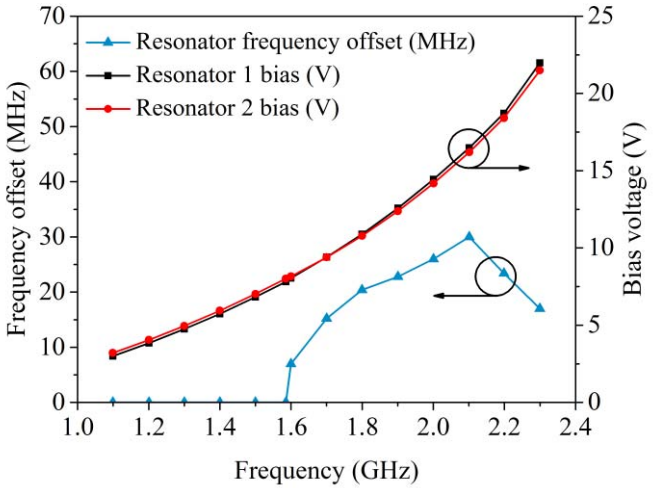

Fig. 22. Plot of varactor bias voltages versus center frequency, and resonator frequency offset versus center frequency. At and below the lower limit of the filter's high-attenuation tuning range, the resonator offset is zero and the resonators are synchronously tuned. Above this lower limit, the resonators are asynchronously tuned to achieve large stopband attenuation.

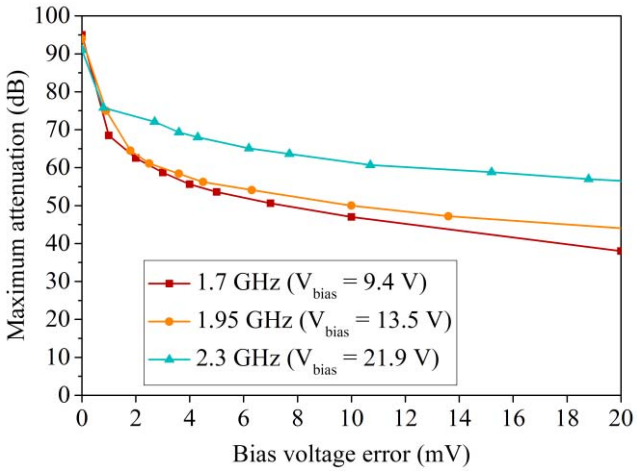

Fig. 23. Effect of error in bias voltage on filter attenuation. Measurements are when filter is tuned to 1.7 GHz, with a nominal varactor bias of 9 V.

levels of stopband rejection are needed over a relatively wide bandwidth, but a wide frequency tuning range is not needed. In between these two extremes, the optimal choice of filter order depends on the stopband bandwidth and tuning range dictated by the specific application, and whether or not the additional complexity, size, and loss of a four-pole filter can be tolerated.

The two bias voltages required to tune Filter B are shown in Fig. 22. The two bias voltages are nearly identical across the whole tuning range. Also shown in Fig. 22 is the frequency offset between the two resonators across its tuning range. It can be seen that at and below the lower limit of the filter's high-attenuation tuning range (∼1.585 GHz), the frequency offset is zero and the resonators are synchronously tuned. Above this lower limit, the resonators are asynchronously tuned in order to realize high levels of stopband attenuation. This is in agreement with the analysis of Section II, in which it was asserted that the frequency offset between the resonators was zero ($B = 0$) at the limits of the filter's tuning range, and that the resonators would be asynchronously tuned ($B \neq 0$) between the upper and lower limits of the filter's tuning range. The maximum frequency offset between the resonators is 30 MHz, or 1.4% at 2.1 GHz.

Lastly, the sensitivity to variations in tuning voltage is examined. Although the filters are able to achieve extremely high levels of stopband attenuation when correctly tuned, errors in tuning voltage will degrade this response. Fig. 23 plots the maximum stopband attenuation versus tuning voltage error for 1.7, 1.95, and 2.3 GHz center frequencies. The sensitivity of stopband rejection to error in tuning voltage decreases as the filter's center frequency is increased. This is to be expected, since a varactor's capacitance becomes less sensitive to change in bias voltage as its bias voltage is increased, due to the nonlinear C-V curve of the varactor. With the relationship between bias voltage error and maximum attenuation known, it is possible to determine how precise the controlling digital-to-analog converter must be in order to achieve a certain guaranteed level of attenuation. For example, it can be noted that at its most sensitive state (1.7 GHz), the maximum attenuation is greater than 40 dB when the tuning voltage error is less than 20 mV. If this voltage error is split between the two varactors, then the required precision for the tuning voltage is 10 mV. Considering that the maximum tuning voltage is 22 V, 10 mV equates to approximately 11 bits of precision. Using similar calculations, it can be determined that 12, 14, and 16 bits of precision are required to achieve guaranteed stopband attenuation levels of 47 dB, 60 dB, and 80 dB, respectively. Though measurements are not shown for bias errors greater than 20 mV, the data could be extrapolated or additional measurements could be taken to determine the suitability of lower-precision voltage sources.

V. Conclusion

In this paper, a detailed analysis of absorptive bandstop filters has been performed, in which theory and simulations are used to derive and demonstrate their operating principles, design considerations, performance tradeoffs, and limitations.

A simple but general step-by-step design procedure has been proposed for the first time, taking into account non-ideal effects such as frequency-dependent couplings and quality factors. The theory and design principles derived are generic and not specific to a given technology, and thus can be used to design a wide variety of absorptive bandstop filters. Several varactor-tuned microstrip filters have been designed to demonstrate the design principles and tradeoffs derived in the paper. A comparison is made between filters with different coupling structures and bandwidths to illustrate their effects on tuning range, and the performance of a two-pole filter is compared to that of a four-pole filter to show its increased selectivity. The filters designed and demonstrated are able to achieve very high levels of stopband isolation (> 90 dB), over as wide as a 1.45:1 tuning range.

REFERENCES

[1] I. F. Akyildiz, W.-Y. Lee, M. C. Vuran, and S. Mohanty, "A survey on spectrum management in cognitive radio networks," *IEEE Commun. Mag.*, vol. 46, no. 4, pp. 40–48, Apr. 2008.

[2] E. J. Naglich, J. Lee, and D. Peroulis, "Tunable bandstop filter with a 17-to-1 upper passband," in *IEEE MTT-S Int. Microw. Symp. Dig.*, Jun. 2012, pp. 1–3.

[3] Y.-H. Cho and G. M. Rebeiz, "0.7–1.0-GHz reconfigurable bandpass-to-bandstop filter with selectable 2- and 4-pole responses," *IEEE Trans. Microw. Theory Techn.*, vol. 62, no. 11, pp. 2626–2632, Nov. 2014.

[4] A. Anand, Y. Liu, and X. Liu, "Substrate-integrated octave-tunable combline bandstop filter with surface mount varactors," in *Proc. IEEE Int. Wireless Symp.*, Mar. 2014, pp. 1–4.

[5] Y.-C. Ou and G. M. Rebeiz, "Lumped-element fully tunable bandstop filters for cognitive radio applications," *IEEE Trans. Microw. Theory Techn.*, vol. 59, no. 10, pp. 2461–2468, Oct. 2011.

[6] I. Reines, S.-J. Park, and G. M. Rebeiz, "Compact low-loss tunable *X*-band bandstop filter with miniature RF-MEMS switches," *IEEE Trans. Microw. Theory Techn.*, vol. 58, no. 7, pp. 1887–1895, Jul. 2010.

[7] W. D. Yan and R. R. Mansour, "Compact tunable bandstop filter integrated with large deflected actuators," in *IEEE MTT-S Int. Microw. Symp. Dig.*, Jun. 2007, pp. 1611–1614.

[8] A. Ghaffari, E. A. M. Klumperink, and B. Nauta, "Tunable N-path notch filters for blocker suppression: Modeling and verification," *IEEE J. Solid-State Circuits*, vol. 48, no. 6, pp. 1370–1382, Jun. 2013.

[9] K. B. Östman *et al.*, "Analysis and design of N-path filter offset tuning in a 0.7–2.7-GHz receiver front-end," *IEEE Trans. Circuits Syst. I, Reg. Papers*, vol. 62, no. 1, pp. 234–243, Jan. 2015.

[10] R. Gómez-García, R. Loeches-Sánchez, D. Psychogiou, and D. Peroulis, "Single/multi-band Wilkinson-type power dividers with embedded transversal filtering sections and application to channelized filters," *IEEE Trans. Circuits Syst. I, Reg. Papers*, vol. 62, no. 6, pp. 1518–1527, Jun. 2015.

[11] D. R. Jachowski, "Narrow-band absorptive bandstop filter with multiple signal paths," U.S. Patent 7 323 955, Jan. 29, 2008.

[12] D. R. Jachowski, "Compact, frequency-agile, absorptive bandstop filters," in *IEEE MTT-S Int. Microw. Symp. Dig.*, Jun. 2005, pp. 1–4.

[13] A. C. Guyette, I. C. Hunter, R. D. Pollard, and D. R. Jachowski, "Perfectly-matched bandstop filters using lossy resonators," in *IEEE MTT-S Int. Microw. Symp. Dig.*, Jun. 2005, pp. 1–4.

[14] D. R. Jachowski and C. Rauscher, "Frequency-agile bandstop filter with tunable attenuation," in *IEEE MTT-S Int. Microw. Symp. Dig.*, Jun. 2009, pp. 649–652.

[15] D. R. Jachowski and A. C. Guyette, "Sub-octave-tunable microstrip notch filter," in *Proc. IEEE Int. Symp. Electromagn. Compat.*, Aug. 2009, pp. 99–102.

[16] D. R. Jachowski, "Octave tunable lumped-element notch filter," in *IEEE MTT-S Int. Microw. Symp. Dig.*, Jun. 2012, pp. 1–3.

[17] T.-C. Lee, J. Lee, E. J. Naglich, and D. Peroulis, "Octave tunable lumped-element notch filter with resonator-Q-independent zero reflection coefficient," in *IEEE MTT-S Int. Microw. Symp. Dig.*, Jun. 2014, pp. 1–4.

[18] M. D. Hickle, M. D. Sinanis, and D. Peroulis, "Tunable high-isolation W-band bandstop filters," in *IEEE MTT-S Int. Microw. Symp. Dig.*, May 2015, pp. 1–4.

[19] M. D. Hickle, M. D. Sinanis, and D. Peroulis, "Design and implementation of an intrinsically-switched 22–43 GHz tunable bandstop filter," in *Proc. IEEE Wireless Microw. Techn. Conf. (WAMICON)*, Clearwater, FL, USA, Apr. 2016, pp. 1–3.

[20] E. J. Naglich, A. C. Guyette, and D. Peroulis, "High-Q intrinsically-switched quasi-absorptive tunable bandstop filter with electrically-short resonators," in *IEEE MTT-S Int. Microw. Symp. Dig.*, Jun. 2014, pp. 1–4.

[21] T. Snow, J. Lee, and W. J. Chappell, "Tunable high quality-factor absorptive bandstop filter design," in *IEEE MTT-S Int. Microw. Symp. Dig.*, Jun. 2012, pp. 1–3.

[22] G. Matthaei, L. Young, and E. M. T. Jones, *Microwave Filters, Impedance-Matching Networks, and Coupling Structures*. Norwood, MA, USA: Artech House, 1980, pp. 430–433.

[23] J.-S. Hong and M. J. Lancaster, *Microstrip Filters for RF/Microwave Applications*, 2nd ed. Hoboken, NJ, USA: Wiley, 2011.

[24] D. M. Pozar, *Microwave Engineering*, 3rd ed. Hoboken, NJ, USA: Wiley, 2005.

[25] A. C. Guyette and E. J. Naglich, "Short-through-line bandstop filters using dual-coupled resonators," in *IEEE Trans. Microw. Theory Techn.*, vol. 64, no. 2, pp. 459–466, Feb. 2016.

[26] J.-S. Hong and M. J. Lancaster, "Cross-coupled microstrip hairpin-resonator filters," *IEEE Trans. Microw. Theory Techn.*, vol. 46, no. 1, pp. 118–122, Jan. 1998.

[27] D. Kajfez and P. Guillon, *Dielectric Resonators*. Atlanta, GA, USA: Noble Publishing Corporation, 1998, pp. 474–480.

Mark D. Hickle (S'11–M'17) received the B.S. degree in electrical engineering from the Missouri University of Science and Technology, Rolla, MO, USA, in 2012, and the Ph.D. degree in electrical and computer engineering from Purdue University, West Lafayette, IN, USA, in 2016. In 2017, he joined BAE Systems, Inc., Merrimack, NH, USA. He was a National Defense Science and Engineering Graduate Fellow with the Purdue University. He was the co-recipient of the first place awards in the RF-MEMS Tunable Filter student design competitions at the 2014 and 2015 International Microwave Symposiums, and was also the co-recipient of the first place award for the 2015 MTT-S Youtube/YouKu video competition.

Dimitrios Peroulis (S'99–M'04–SM'15–F'17) received the Ph.D. degree in electrical engineering from the University of Michigan, Ann Arbor, MI, USA, in 2003. Since 2003, he has been with Purdue University, West Lafayette, IN, USA, where he is currently a Professor of electrical engineering and the Deputy Director of the Birck Nanotechnology Center. His current research projects are focused on the areas of reconfigurable electronics, RF microelectromechanical systems (MEMS), and sensors in harsh environment applications. He has been a key contributor on developing very high quality RF MEMS tunable filters in mobile form factors. He has co-authored over 270 journal and conference papers. He has also been involved in the investigation of failure modes of RF MEMS and MEMS sensors through the Defense Advanced Research Projects Agency, MEMS/Nanoelectromechanical Systems Science and Technology Fundamentals Program, Phases I and II and the Center for the Prediction of Reliability, Integrity and Survivability of Microsystems funded by the National Nuclear Security Administration.

Dr. Peroulis was the recipient of the National Science Foundation CAREER Award in 2008, the Outstanding Young Engineer Award of the IEEE Microwave Theory and Techniques Society in 2014, and the Outstanding Paper Award of the IEEE Ultrasonics, Ferroelectrics, and Frequency Control Society (Ferroelectrics Section) in 2012. His students have been the recipient of numerous Student Paper Awards and other student research-based scholarships. He is a Purdue University Faculty Scholar and has also received ten teaching awards including the 2010 HKN C. Holmes MacDonald Outstanding Teaching Award and the 2010 Charles B. Murphy award, which is Purdue University's highest undergraduate teaching honor.